Performance of mixed mesoporous silica Si(Mes)-perovskite (P) to remove hydroxybenzene in aqueous solution — effect of parameters influencing the adsorption efficiency

Moussa Abbas[a,*], Tounsia Aksil[a], Mohamed Trari[b]

[a]Laboratory of Soft Technologies and Biodiversity, Faculty of Sciences, University M'hamed Bougara, Boumerdes 35000, Algeria, Tel. +213 552408419; Fax: +213 21 24 80 08; emails: moussaiap@gmail.com (M. Abbas), tounsiaiap@gmail.com (T. Aksil)
[b]Laboratory of Storage and Valorization of Renewable Energies, Faculty of Chemistry (USTHB), BP 32-16111 Algiers, Algeria, email: mtrari@usthb.dz (M. Trari)

ABSTRACT

Mesopores are materials with pore diameters between 2 and 50 nm, are used in several fields such as catalysis, chromatography, adsorption, etc. This study focuses on the potential use of mesoporous Si(Mes) and perovskite (P) as adsorbents, their ability to remove hydroxybenzene from aqueous solutions and the possibilities of elimination of a certain class of phenolic compounds, whose chemical structures of which contain functions capable of interacting on the surface of the supports. The adsorbent was characterized by Brunauer–Emmett–Teller, Fourier-transform infrared spectroscopy and X-ray diffraction methods. Batch adsorption experiments were undertaken to assess the effect of physical parameters on the hydroxybenzene removal efficiency. It has been observed that under optimized conditions (pH 4; adsorbent dose 1 g L^{-1}; agitation speed 200 rpm; contact time 90 min); up q_{max} of 4.210 g of hydroxybenzene/g adsorbent at 25°C were removed from the solution. The adsorption by the adsorbent follows a pseudo-second-order kinetic model with a determination coefficient (R^2) of 0.999; which relies on the assumption that the physisorption may be the rate-limiting step. The adsorption at different temperatures has been used for the determination of thermodynamic parameters, the negative free energy ($\Delta G°$) and positive enthalpy ($\Delta H°$) indicate that the overall adsorption is spontaneous and endothermic, while the negative value ($\Delta S°$) states clearly that the randomness increases at the solid-solution interface during the phenol adsorption onto Si(Mes)-(P), indicating that some structural exchange may occur among the active sites of the adsorbent and the ions.

Keywords: Perovskite; Mesoporous; Silica; Isotherm; Removal; Modeling; Kinetics

1. Introduction

Many wastewaters contain significant levels of organic contaminants, which are toxic or otherwise undesirable because they generate odor, unsightly color, foaming, etc [1]. Among the different organic pollutants of aquatic ecosystems, the phenols, especially chlorinated, are considered as priority pollutants since they are harmful to plants, animals, and humans, even at low concentrations [2]. The problem of water pollution is a big challenge in time, due to rapid population growth, water demand every day higher [3]. The discharge of the wastewater containing large amounts of organic contaminants represents a serious risk to the general population [4]. Wastewater containing phenolic compounds implies serious discharge problems, due to their poor biodegradability, high toxicity, and accumulation in the environment. Phenols are introduced into surface water from industrial

---

* Corresponding author.

effluents, such as plastic, leather, paint, rubber, pharmaceuticals, petrochemicals and pesticides, among others [5–7]. It is a fact that hydroxybenzene and its derivatives in natural water sources represent a threat to human health and water quality [8] because of their high toxicity and carcinogenicity even at low concentrations. Environmental Protection Agency (EPA) regulations demand lowering hydroxybenzene content in wastewater to less than 1 mg L^{-1} [9]. There are many methods for the treatment of phenolic compounds, but the adsorption remains one of the most widely used due to its simple implementation and low operation cost. Research has been carried out to find effective materials for the treatment of phenolic wastes and there is a necessity to develop new adsorbents for their elimination and the activated carbon is among the most effective adsorbents [10,13]. Ideally, removal processes must be simple, effective and inexpensive and several techniques have been suggested, including biological and physic-chemical methods. However, adsorption has been proven as an effective and reliable method. Its major advantages for the control of water pollution are less investment in terms of development cost, simple design, easy operation, free from the generation of toxic substances, and easy and safe recovery of the adsorbent as well as adsorbate materials. Activated carbons are widely used in the water treatment which enables the adsorption of both cationic and anionic pollutants. Recently, the use of agricultural waste as activated carbon precursors has proved to be renewable and less expensive. Therefore, the research has been focused on the preparation of activated carbons based on agricultural wastes and lignocelluloses materials such as coffee waste [11], date pits [12], apricot stone [13–15]. On the other hand, the inorganic compounds crystallizing in perovskite structure are widely used in modern electronics because of their high *Chenopodium album* [16], rice straw and biomass material [17,18] dielectric permittivity, high piezoelectric coefficient of their ferroelectricity, semiconductivity, thermoelectricity, catalytic activity and photocatalysis. These properties lend themselves to many applications in optoelectronics, dielectric for the manufacture of multilayer capacitors and transducers. In this study, it was necessary to understand how the phenol interacts with the adsorbent during discoloration and to describe the processes involved in these interactions. For this purpose, parametric research of the adsorption has been undertaken by studying the effect of several significant parameters on the decolorizing power of the material particularly the contact time, the adsorbent dose, pH, stirring speed and temperature. Furthermore, the adsorption isotherms were performed and their modeling was achieved by applying known models. The performances of adsorbent on the phenol adsorptions were evaluated using equilibrium, kinetic and thermodynamic studies.

2. Materials and methods

2.1. Preparation of phenol solutions

Phenol solutions were used as a surrogate indicator to simulate industrial wastewater and to evaluate the adsorption capacity of Si(Mes)-(P). The characteristics and molecular structure of phenol (hydroxybenzene) are illustrated in Table 1; Phenol was purchased from Merck (India) Ltd.

The solutions were prepared using crystallized phenol and distilled water to have a good reproducibility of adsorption results. We prepared a large volume (1 L) of stock solution (1,000 mg L^{-1}); then it was diluted to prepare standard solutions to study the effect of the initial dye concentration. The phenol concentration was titrated with a UV-Visible spectrophotometer (λ_{max} = 270 nm). The initial pH of the solution was adjusted by using HCl or NaOH solution (0.1 M).

2.2. Preparation of mesoporous silica Si(Mes)

Generally, during the synthesis of mesoporous materials, four major elements are used: (a) anionic, cationic, nonionic or neutral surfactant molecule (structuring agent) for directing the final structure of the material. (b) Source of silica (fumed silica, sodium silicate, etc). (c) Solvent (water, ethanol, etc). (d) Acidic, basic or neutral catalyst according to the desired synthesis. The formation of the mesoporous material can be explained as follows: the surfactant molecules with a positive, negative or neutral charge, a hydrophilic head, and a long hydrophobic chain. When the solutions containing the surfactant molecules and the silica source are mixed, three types of interaction can take place: organic–inorganic, organic–organic and inorganic–inorganic. In order to minimize the free energy of the system, we observe the formation of organic–inorganic interface (ion exchange), the organization of organic micelles with each other so as to form a cubic, hexagonal or lamellar structure and the condensation of the inorganic phase [19].

2.3. Syntheses of monoporous silica Si(Mes)

Si(Mes) was prepared using nonionic surfactant glycols based polymer, more particularly the three-block copolymer consisting of an assembly of polyethylene glycol-polypropylene glycol-polyethylene glycol units such as Pluronics. The Si(Mes) type samples used in this work were prepared from the protocol described by the Roggenbuck Method

Table 1
Physicochemical properties of phenol

Parameter	Value
Melting temperature (°C)	43
Boiling temperature (°C)	182
Auto-ignition temperature (°C)	715
Saturation vapor pressure at 20°C	47 Pa
Half life time in the air (h)	20
Half life time in water (h)	55
Solubility (g L^{-1})	97
Volumic mass (g cm^{-3})	1.073
Chemical formula	C_6H_6O
Molar mass (g mol^{-1})	94.1112 ± 0.0055
Composition	C: 76.57%; H: 6.43%; O: 17%
Dipolar moment (D)	1.220 ± 0.008
Molecular diameter (nm)	0.55
International Union of Pure and Applied Chemistry	Hydroxybenzene

[20], 12 g of commercial Pluronic was dissolved in 360 g of distilled water and 43 g of HCl (32% wt.%). The solution was stirred at 35°C to allow the complete dissolution of the structurant. 24 g of tetraethyl orthosilicate was then added under sustained agitation. The molar gel composition obtained was fixed at 1, tetraethyl orthosilicate: 0.018 commercial Pluronic: 3.3 HCl: 187 H_2O. The solution was stirred for 24 h at 35°C, transferred into an autoclave for aging during 24 h at 50°C, 100°C or 140°C to obtain respective pore diameters of the order of 6, 8 and 10 nm. After aging, the solid was recovered by filtration, washing and drying at 80°C for 12 h. The solid was finally calcined at 550°C under airflow for 3 h (Fig. 1).

2.4. Synthesis of massive perovskites (P)

This method consists of dissolving masses of precursor (metal and lanthanum nitrates) corresponding to the desired percentages of the solid in a known quantity of distilled water. After the dissolution of nitrates, glycine ($H_2NCH_2CO_2H$) fuel was added as a complexing agent (NO_3^-/glycine = 1) [21] while maintaining agitation, water was evaporated by increasing the temperature to 100°C. After that, a dry gel was obtained. Then, the temperature was increased to 280°C to allow the self-burning of glycine. All samples were calcined at 600°C to remove the residual carbon from incomplete glycine combustion. The crystallographic structure of perovskite is represented in Fig. 2 and the characteristics are as follows (lattice: cubic P (idealized structure), 1 ABO_3 per mesh, pattern: (A^{+2} to (0, 0, 0); B^{4+} to (1/2, 1/2, 1/2); $3O^{2-}$ to (1/2, 0, 0), (0, 1/2, 0), (0, 0, 1/2).

2.5. Characterizations

The Fourier-transform infrared spectroscopy (FTIR) analysis was carried out with a spectrometer (BRUKER VERTEX 70) with a resolution of 4 cm^{-1} where the band range varies from 400 to 4,000 cm^{-1}, controlled by a microcomputer (Bruker Corporation, Germany). To analyze our samples, we used the method of pelletization with KBr of spectroscopic quality. It consisted of intimately mixing the solid substance with a quantity of KBr, in an agate mortar and finally compressed in a vacuum hydraulic press. The material was transformed under a cold flow into a transparent pellet, the latter was then placed in the path of the light beam.

The X-ray diffraction (XRD) patterns were obtained with a Philips PW 1730 diffractometer equipped with Cu-Ka radiation (40 kV, 30 mA) (Philips Research Eindhoven, The Netherlands).

The specific surface area of sample clay was determined by the Brunauer–Emmett–Teller (BET) method by using Quantachrome Asi Quin (Corporate Headquarters, Boynton Beach, Florida, USA), Automated Gas Sorption Analyzer (Quantachrome Instrument Version 2.02, using the ASAP 2010 Micromeritics Equipment, Corporate Headquarters, Boynton Beach, Florida, USA).

2.6. Adsorption studies

The effects of the initial phenol concentration (C_0: 20–100 mg L^{-1}), solution pH (1.5–5), adsorbent dose (0–50 g L^{-1}) and temperature (293–333 K) on the phenol adsorption were investigated in batch mode for variable specific periods (0–120 min) under constant agitation (200 rpm). The phenol solutions were made up of dissolution of the stock solution (1 g L^{-1}) of phenol (99%) in distilled water, to the required concentration; pH was adjusted with HCl or NaOH (0.1 mol L^{-1}). For the kinetic studies, desired quantities of Si(Mes)-(P) were contacted with 50 mL of phenol solutions in Erlenmeyer flasks and placed on a rotary shaker at 200 rpm, the aliquots were withdrawn at regular times and subjected to vigorous centrifugation (3,000 rpm and 10 min). The remaining phenol concentration was titrated with a PerkinElmer LAMBDA 365 UV/Vis Spectrophotometer, (India) model 550S (λ_{max} = 270 nm). The (%) removal of phenol adsorbed R_t (%) by Si(Mes)-(P) was calculated from the relation:

$$R_t = \frac{C_0 - C_t}{C_0} \times 100 \tag{1}$$

where C_t is phenol concentration (mg L^{-1}) at the time (*t*). Due to the inherent bias resulting from the transformation that overlaps toward a diverse form of parameters estimation errors and fits distortion, several mathematically rigorous
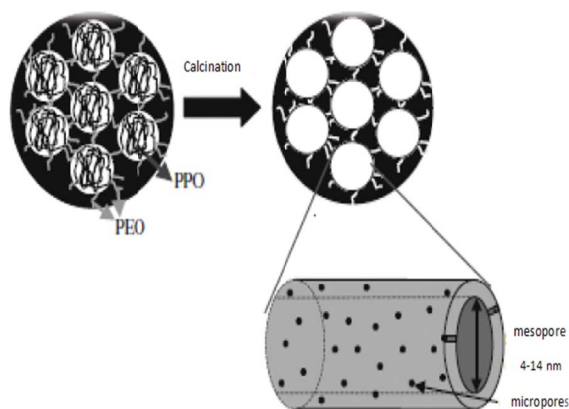

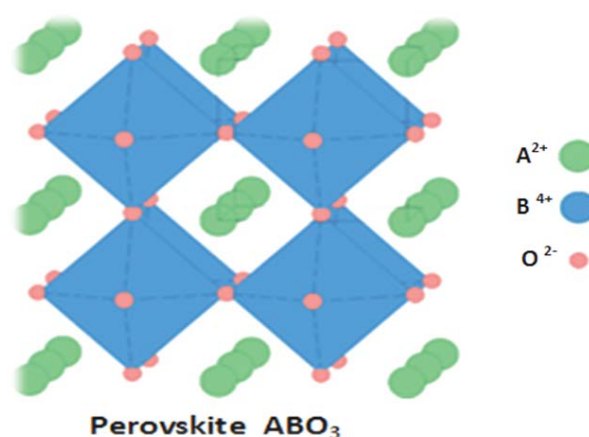Fig. 1. Structure of Si(Mes) before and after heat treatment at 550°C.

Fig. 2. Crystal structure of perovskite ABO_3.

error functions. Because of the inherent bias resulting from the linearization of isotherm models, the non-linear regression Chi-squares (χ^2) Eq. (2) the test was used as a criterion for the fitting quality. A smaller χ^2 value indicates a better curve fitting [22–24].

$$\chi^2 = \sum_1^N \frac{\left(q_{e,\exp} - q_{e,\text{cal}}\right)^2}{q_{e,\text{cal}}} \tag{2}$$

where $q_{e,\exp}$ (mg g^{-1}) is the uptake experimental, $q_{e,\text{cal}}$ the calculated value of uptake using a model (mg g^{-1}) and N the number of data points in the experiment.

2.7. Effect of different parameters for the adsorption processes

2.7.1. Effect of pH

The pH of the solution is one of the most sensitive parameters of adsorption, particularly on its capacity. The influence of pH on the phenol adsorption on the mesoporous material was carried out with solutions of phenol (25 mg L^{-1}) placed in contact with 0.2 g of the adsorbent Si(Mes)-(P) and with pHs varying between 1.5 and 5. Fig. 3 shows that the adsorption efficiency of phenol increases with increasing the solution pH. The best performance (~70%) was obtained at pH 4. In an acid medium, the positive charge is dominant on the adsorbent surface and thus a substantially high electrostatic attraction exists with the negative charges of formed phenolates, thus favoring the adsorption (Fig. 4).

Conversely, high pH causes the reduction of the electrostatic repulsion, due to the reduction of positive charge density on the active sites of the adsorbent resulting in a decreased adsorption of the phenol ions; the OH$^-$ ions compete with the phenol ions to occupy the active sites of the adsorbent surface. The maximum adsorption is obtained at pH 4, which allows us to retain this optimal value for the rest of the parametric study.
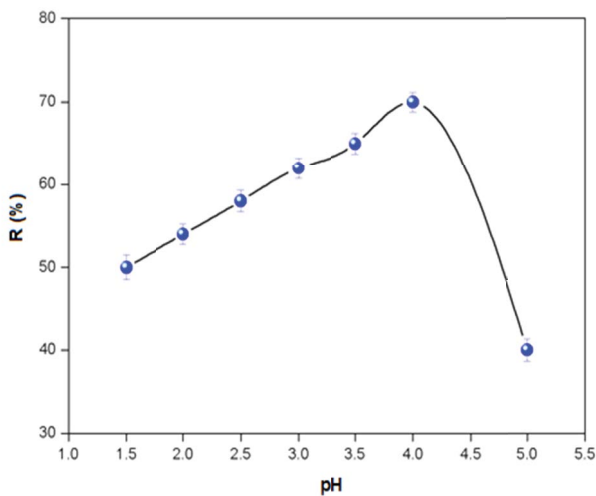
2.7.2. Effect of contact time on phenol removal efficiency

The influence of the contact time on the adsorption of phenol by the mesoporous is also an important step because it enables us to determine the required duration to reach equilibrium. The results obtained are reported in Fig. 5, which illustrates the evolution of the removal efficiency of the phenol as a function of time. We can deduce that the adsorption is done in three steps:

- Accelerated adsorption of the phenol in solution due to the presence of free sites on the surface of the adsorbent particles, which reflects the linear increase in the adsorption capacity over time. This step lasts 20 min. under the intended conditions of use.
- Reduction in the adsorption rate resulting in a very small increase in the capacity due to the decrease in the amount of phenol in solution and the number of available sites; this step lasts from 20 to 60 min.
- Stability of the adsorption capacity observed from 60 min, due to the almost total occupancy of adsorption sites, which results in a level.

The phenol ions are adsorbed initially on the external adsorbent surface area which makes the adsorption rate easy and fast. Once the external surface is saturated, the phenol ions entered inside the pores and absorb on the internal surface of particles and such a phenomenon takes a relatively long time. This may be attributed to an increase of the driving force due to the concentration gradient with increasing C_0 in order to overcome the mass transfer resistance of phenol ions between the aqueous and solid phases. Therefore, a higher initial phenol concentration C_0 increases the adsorption capacity; similar results were obtained in the literature [25].

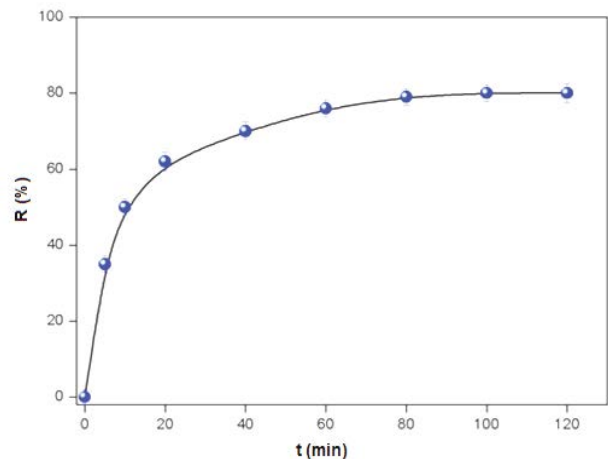Fig. 4. Phenol dissociation equilibrium in an aqueous medium.

Fig. 3. Influence of pH on phenol removal efficiency by Si(Mes)-(P).

Fig. 5. Effect of contact time on phenol removal efficiency.

2.7.3. Effect of initial pollutant concentration on removal efficiency

For this present experiment, 0.2 g samples of the modified support were contacted with organic solutions (50 mL), at pH 4 and at different phenol concentrations C_0. The results (Fig. 6) show that the phenol extraction rate decreases with increasing C_0. This effect can be explained as follows; at low concentrations, the adsorption of phenolic ions occurs at high energy sites. As C_0 increases, high energy sites are saturated and the adsorption begins at lower energy sites, resulting in decreased adsorption efficiency.

2.7.4. Effect of agitation speed

The effect of the stirring speed in the range (100–700 rpm) on the adsorption capacity of phenol onto Si(Mes)-(P) is also studied. The optimal capacity is obtained for a speed of 200 rpm, which gives the best homogeneity of the mixture suspension. Above 200 rpm, a desorption phenomenon occurs. Therefore, the optimal rotational speed of 200 rpm is selected for subsequent tests.

2.7.5. Effect of adsorbent dose

The effect of the concentration of the modified support on the retention of phenol ions by Si(Mes)-(P) was studied at optimal pH (=4) and 2 h of contact; the dose ranges from 0 to 45 g mg^{-1}. Fig. 7 illustrates the evolution of the extraction yield as a function of the concentration of the mesopore support, clearly reveals a gradual increase in the extraction rate until the appearance of a plateau from Si(Mes)-(P); this is due to the increased exchange surface. Therefore, this optimal adsorbent dose will be used for the next parametric study.

3. Results and discussion

3.1. BET surface area and pore size

The specific surface area (S_{sp}) of the sample clay was determined by the BET method. S_{sp} and pore structure of the activated carbons were characterized by N$_2$ adsorption–desorption isotherms at −196°C, the isotherm is identical to type II at low pressures and S_{sp} was determined by the BET equation. The external surface area, micropore area and micropore volume were calculated by the *t*-plot method. The total pore volume was evaluated from the liquid volume of N$_2$ at high relative pressure near unity 0.99. The mesopore volume was calculated by subtracting the micro-pore volume from the total volume. The pore size distribution was determined using the density functional theory model. The textural characteristics of Si(Mes) and Si(Mes)-(P) are presented in Table 2.

3.2. Infrared spectroscopy study

The samples were analyzed by the FTIR spectroscopy for the identification of natural minerals [26]. It is a useful technique to qualitatively determine the characteristic functional groups of the adsorbents; it is also a physical method of structural analysis. It reveals the nature of interatomic

bonds in a molecule and identifies the functional groups [27]. The FTIR spectra of the solids before adsorption show, the presence of silicate network characteristic bands. The band centered at 454 cm^{-1} is assigned to the Si–O bond, while the band at 802 is due to Si–O. The band located between 1,500 and 2,000 cm^{-1} corresponds to the deformation of Si–OH group while the broadband at 3,441 cm^{-1} with a low intensity ascribed to silanol Si–OH is observed for the solids before adsorption. The spectrum after adsorption (Fig. 8) shows a broad band centered at 3,446 cm^{-1} characteristic of phenol, clearly confirming its adsorption on the support.

3.3. Structural analysis of Si(Mes) and Si(Mes)-(P) by XRD

At low angles of support (Fig. 9) allowed the detection of three well-resolved reflection peaks at 2θ between 1° and 2°, characteristic of the reflection of (100), (110) and (200) of the hexagonal structure P6mm of the pores.
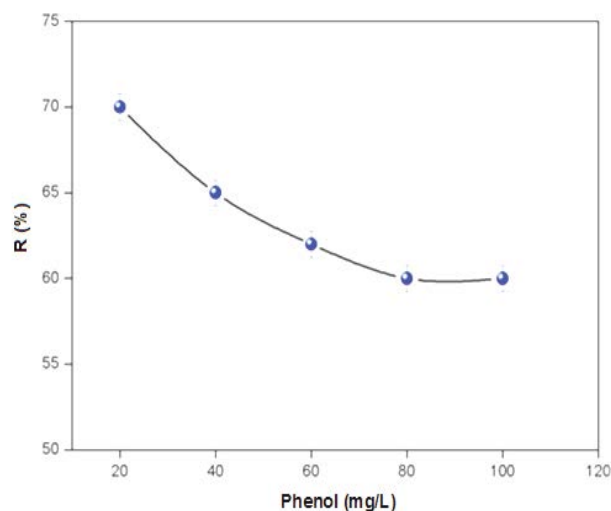

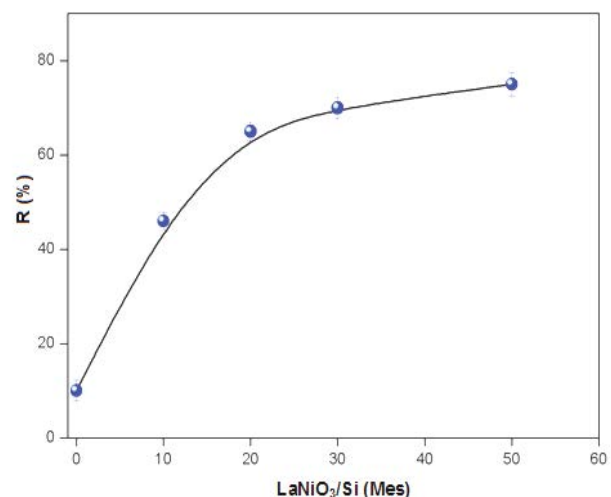Fig. 6. Effect of initial pollutant concentration on removal efficiency.

Fig. 7. Influence of the concentration of the adsorbent.

Table 2
Textural characteristics of Si(Mes) and Si(Mes)-(P)

Compose	Surface area ($m^2\,g^{-1}$)	Pore diameter (nm)	Pore volume ($cm^3\,g^{-1}$)
Si(Mes)	426	9.6	1.23
Si(Mes)-(P)	450	10.3	1.42

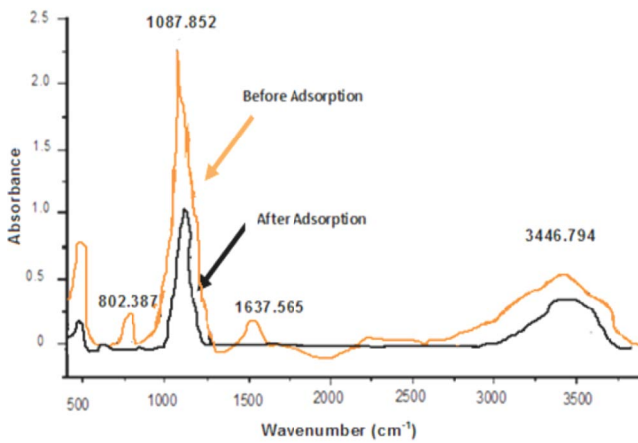Si(Mes): mesoporous silicate; (P): perovskite ABO_3 ($LaNiO_3$)

Fig. 8. FTIR spectra of the mixture Si(Mes)-(P) before and after adsorption in the range 500–4,000 cm^{-1}.
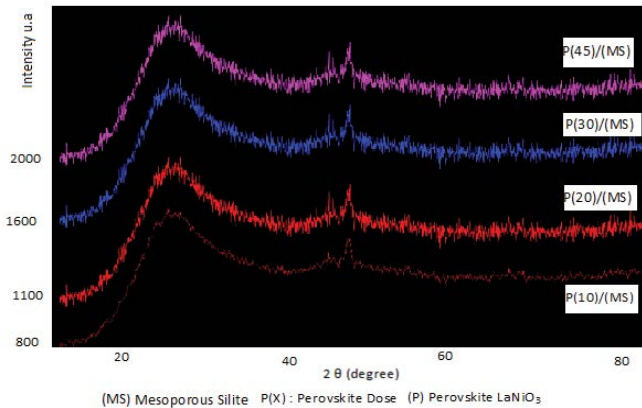

Fig. 9. Low-angle X-ray diffraction spectrum of Si(Mes) and perovskite (P).

Nevertheless, the shift of reflection peak at low 2θ values with the impregnation-auto-combustion cycle leads to a slight increase in the mesh parameters. The presence of the three reflections of the nanocomposites derived from Si(Mes) suggests that the pore structure is not or slightly affected by the formation of mixed oxide particles. Wide XRD angles of the analyzed solids revealed the formation of mixed oxide nanocrystals for all synthesized nanocomposites. Comparing with the perovskite mass, the analysis of nanocomposites does not allow the detection of characteristic reflections of this structure. Indeed, the low reflection at 2θ = 42.9° corresponds to the single metal oxide.

3.4. Adsorption kinetic study

In order to elucidate the phenol adsorption on Si(Mes)-(P), particularly the rate-controlling step, the adsorption data were analyzed by the pseudo-first-order model:

The pseudo-first-order equation [28] is given by:

$$\log\left(q_e - q_t\right) = \log q_e - \frac{K_1}{2.303} \times t \tag{3}$$

and pseudo-second-order model [29]:

$$\frac{t}{q_t} = \frac{1}{K_2 \cdot q_e^2} + \frac{1}{q_e} \cdot t \tag{4}$$

where q_t (mg g^{-1}) is the amount of adsorbed phenol on Si(Mes)-(P) at time t (min); K_1 (min^{-1}) and K_2 (g mg^{-1} min^{-1}) are the pseudo-first-order and pseudo-second-order kinetics constants respectively. The slope and intercept of the plots $\ln(q_e - q_t)$ vs. t are used to determine the constants K_1 and q_e while the slope and intercept of the plot of t/q_e vs. t permit to determine the constants K_2 and q_e; the rate constants the corresponding determination coefficients are summarized in Table 3. For the pseudo-first-order kinetic (Fig. 10a), the experimental data deviate from the linearity as evidenced by the low values of q_e and C_0. Therefore, this model is inapplicable in the present system. By contrast, the $q_{e,cal}$ value determined from the pseudo-second-order kinetic model agrees with the experimental data (Fig. 10b) and the model suggests that the phenol adsorption onto Si(Mes)-(P) is based on chemical reaction, involving an exchange of electrons between adsorbent and adsorbate. In the chemisorption, the phenol ions are attached to the adsorbent surface by chemical bonds and tend to find sites that maximize their coordination number with the surface. The rate-limiting step is also an important factor to

Table 3
Pseudo-first-order and pseudo-second-order model constants and determination coefficients for phenol adsorption

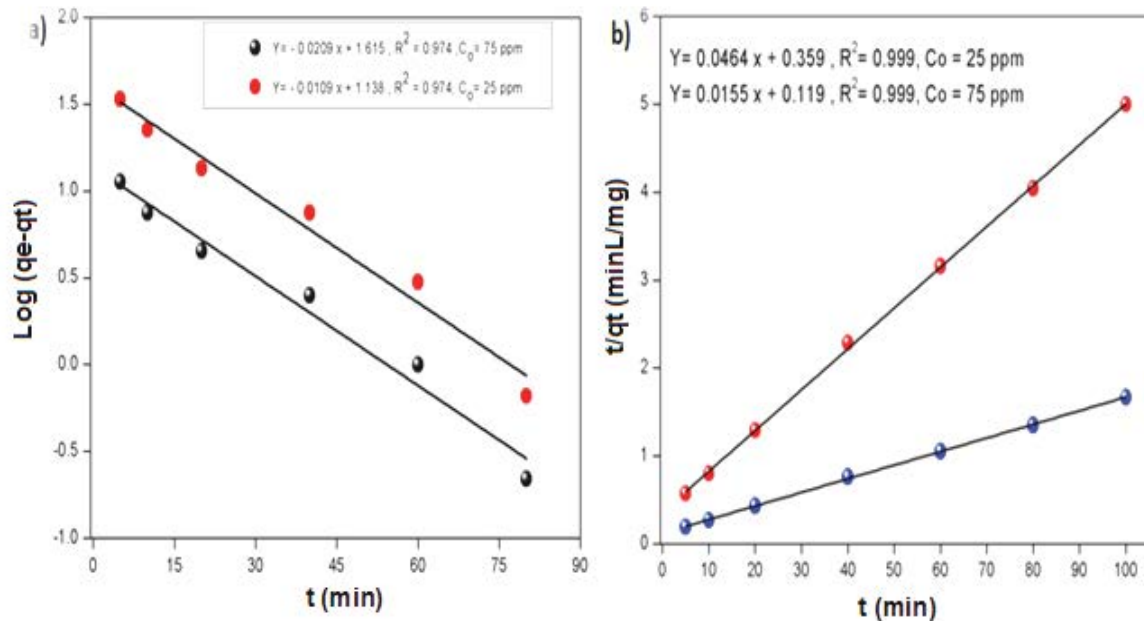|	Pseudo-second-order kinetic					Pseudo-first-order kinetic					
C_0	$q_{e,exp}$	$q_{e,cal}$	K_2	R^2	χ^2	$\Delta q/q$	$q_{e,cal}$	K_1	R^2	χ^2	$\Delta q/q$
25	20	21.59	6.023×10^{-3}	0.999	0.104	7.37	13.74	4.8×10^{-2}	0.974	2.852	31.30
75	60	64.52	2.018×10^{-3}	0.998	0.316	7.01	41.20	2.5×10^{-2}	0.972	8.579	31.33

Fig. 10. Adsorption kinetics (a) pseudo-first-order kinetics and (b) pseudo-second-order kinetics.

Table 4
Parameters of the adsorption isotherms for phenol onto Si(Mes)-(P)

Model	Langmuir	Freundlich	Temkin
	$q_{max} = 4{,}210$ mg g^{-1}	$n = 0.7415$	$B_T = 0.621$
	$K_L = 0.00504$ L mg^{-1}	$K_F = 7.558$ mg g^{-1}	$A_T = 86.488$ L mg^{-1}
			$\Delta Q = 168{,}085.5$ kJ mol^{-1}
R^2	0.9903	0.9685	0.9988

consider in the adsorption. The phenol and silanol groups of the adsorbent surface area in a protonated form, making it possible that the phenol is adsorbed by hydrogen bonding (Fig. 11). This mechanism is similar to that reported for the adsorption of phenol onto the surface of silica [30].

3.5. Adsorption isotherms

Several models are reported in the literature to describe the experimental adsorption data; the analysis of isotherms is important to develop equations that represent the results that could be used for design purposes. In this study, three models (Langmuir, Freundlich and Temkin) were used to describe the relationship between the amount of adsorbed phenol and its equilibrium concentration; the isotherm is represented in Fig. 12. According to Langmuir [31], there is a fixed number of homogeneous active binding sites on the adsorbent surface, and the interaction adsorbent/adsorbate stops once the active binding sites are saturated. This isotherm explains the monolayer adsorption process.

The Langmuir isotherm is expressed as follows:

$$\frac{1}{q_e} = \frac{1}{q_m \cdot K_L} C_e + \frac{1}{q_m} \tag{5}$$

where C_e is the equilibrium concentration (mg L^{-1}), q_{max} the monolayer adsorption capacity (mg g^{-1}) and K_L the constant related to the free adsorption energy (Langmuir constant, L mg^{-1}). Fig. 13a shows a linear plot for the adsorption isotherm. The equilibrium parameter for the isotherm called separation factor (R_L), expressed by the relation:

$$R_L = \frac{1}{1 + K_L C_0} \tag{6}$$

R_L indicates the shape of the isotherm: $R_L > 1$ is unfavorable, $R_L = 1$ is linear, $R_L = 0$ is irreversible and finally $0 < R_L < 1$ is favorable.

The linear form of Freundlich isotherm is given by equation [32]:

$$\ln q_e = \ln K_F + \frac{1}{n} \ln C_e \tag{7}$$

where K_F is the constant indicative of the adsorption capacity of the adsorbent (L g^{-1}). $1/n$ varies between 0 and 1 and shows the adsorption intensity of phenol; it is useful to describe the removal ability of the adsorbent. The plot $\ln q_e$ vs. $\ln C_e$ (Fig. 13b) gives a straight line whose slope and intercept

provides the values of n and K_F respectively. The adsorbent can adsorb the phenol only from its high concentration solution if $1/n$ is higher than 1. On the other hand, the value of $1/n < 1$ suggests the applicability of the adsorbent over the entire concentration range.

The Temkin adsorption isotherm [33] indicates the adsorption of adsorbate occurs on energetic and non-equivalent adsorption sites on the adsorbent surface and the adsorption takes place on the more energetic adsorption sites at first [34]. There is a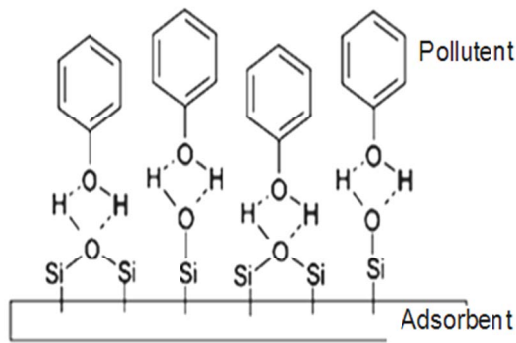 linear increase in the heat of adsorption with the coverage of phenol molecules over the adsorbent surface; the linear form is expressed as:

$$q_e = B_T \ln C_e + B_T \ln A_T \qquad (8)$$

where $B_T = RT/b$.

Fig. 11. Proposed adsorption mechanism of phenol molecules onto the surface of the adsorbent.
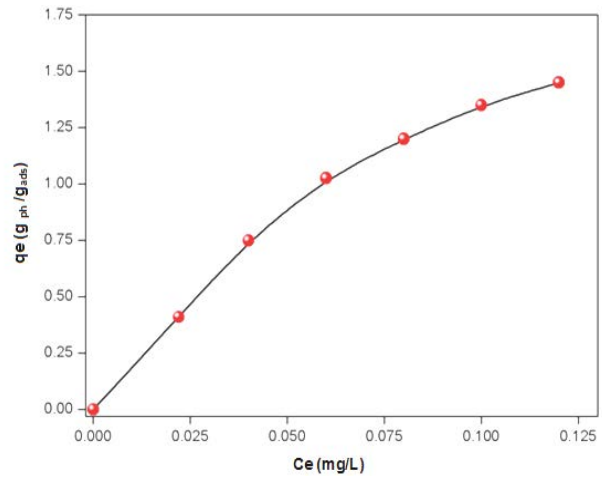

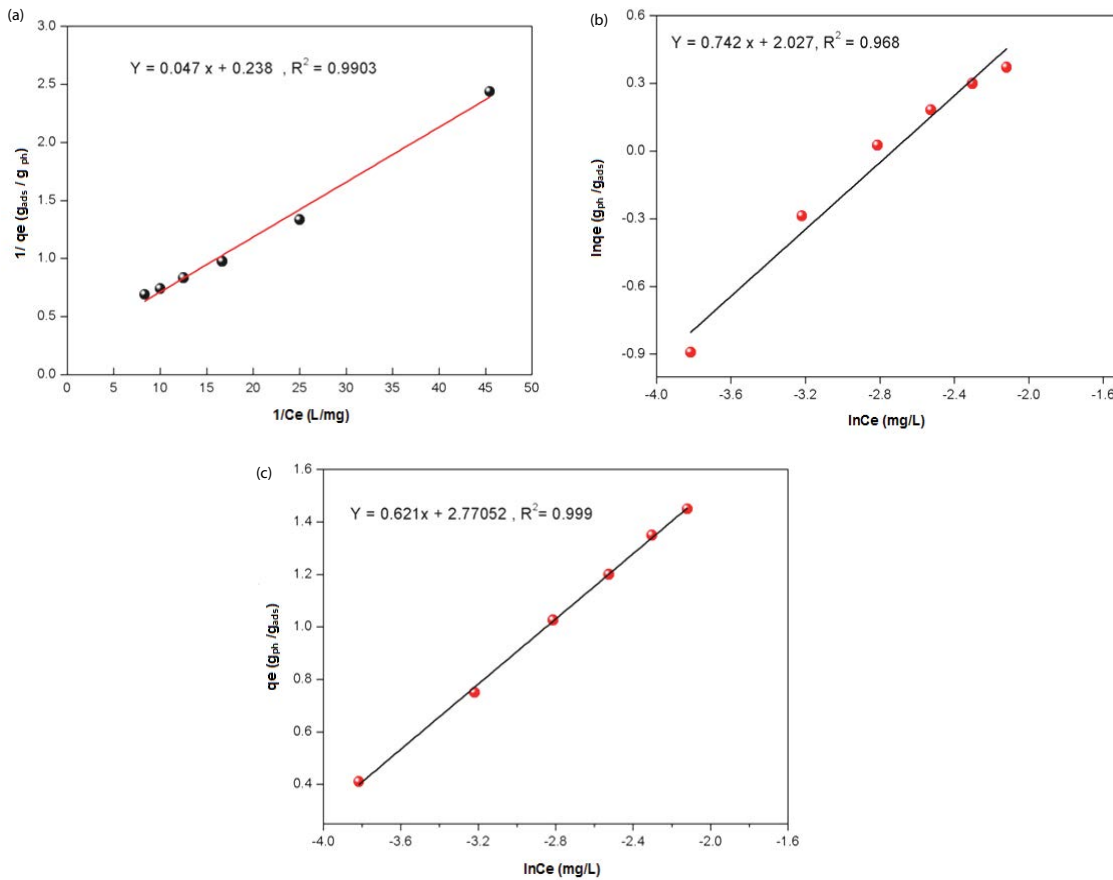Fig. 12. Pollutant adsorption isotherm under optimal conditions.

Fig. 13. (a) Isotherm modeling according to (a) Langmuir's, (b) Freundlich, and (c) Temkin theoretical model.

Table 5
Thermodynamic functions $\Delta G°$, $\Delta S°$ and $\Delta H°$ of phenol adsorbed on the Si(Mes)-(P)

T (K)	$1/T$ (K^{-1})	lnK_d	$\Delta H°$ (kJ mol^{-1})	$\Delta S°$ (J mol^{-1} K^{-1})	$\Delta G°$ (J mol^{-1})
293	0.0030	0.0734			−52.47
303	0.0031	0.0607			−90.17
313	0.0032	0.0480	1.052	3.77	−127.87
323	0.0033	0.0353			−165.67
333	0.0034	0.0227			−203.27

The constant B_T (L mg^{-1}) is related to the adsorption heat, A_T (mg L^{-1}) a constant of the Temkin isotherm, b (J mol^{-1}) the energy constant of the isotherm, R (8.314 J K^{-1} mol^{-1}) the gas constant and T(K) the absolute temperature. Fig. 13c shows a linear plot of the Temkin adsorption isotherm. The calculated parameters, characteristics of each model are given in Table 4. It can be seen that the Langmuir isotherm fits better than the other two others with a higher determination coefficients R^2 very close to unity, while the smaller χ^2 values confirm the better curve fitting. For all studied temperatures, we can note that the evolution of R_L which lies between 0 and 1, indicating that the phenol adsorption onto Si(Mes)-(P) is a favorable process.

3.6. Thermodynamic study

The adsorption reaction of phenol molecules on the adsorbent surface implies a variation of the free energy ($\Delta G°$) between the initial and final states. The adsorption capacity of Si(Mes)-(P) increase with increasing temperature (293–333 K), indicating that the adsorption is favored at high temperature. The thermodynamic functions $\Delta G°$, $\Delta H°$, and entropy $\Delta S°$) are calculated from the following equations [35]:

$$\Delta G° = \Delta H° - T\Delta S° \tag{9}$$

$$\Delta G° = -RT \ln K_d \tag{10}$$

where K_d is the distribution coefficient ($=q_e/C_e$). The apparent enthalpy ($\Delta H°$) and entropy ($\Delta S°$) of the adsorption are calculated from adsorption data at different temperatures using the van't Hoff Eq. (11) as follows:

$$\ln K_d = -\frac{\Delta H°}{RT} + \frac{\Delta S°}{R} \tag{11}$$

The adsorption is described by the functions $\Delta H°$, $\Delta S°$, and $\Delta G°$ due to the transfer of solute to the solid-liquid interface. $\Delta H°$ and $\Delta S°$ are calculated by plotting lnK_d as a function of $1/T$ (Fig. 14) [36], the values are presented in Table 5. The positive enthalpy ($\Delta H°$) confirm that the phenol adsorption on the adsorbent sites is endothermic and indicates by the increase of the adsorbed quantity with raising the temperature and that the molecule/particle interactions are of physical nature ($\Delta H° < 40$ kJ mol^{-1}) which confirms that the bonds are of the electrostatic type (hydrogen bond).

The efficiency of Si(Mes)-(P) for the phenol adsorption presented in this work is positively compared with other adsorbents which have been reported in the literature (Table 6), the maximum adsorption capacity is used as a comparative parameter. Our adsorption capacity shows that Si(Mes)-(P) is one of the good adsorbents and could be used for the preparation of activated carbons.

Table 6
Comparison of maximum adsorbed capacities for phenol with literature data

| Adsorbent	q_{max} (mg g^{-1})	Reference
Clay pyrophyllite (PB)	11.49	[36]
Treated clay pyrophyllite (PT)	13.70	
Natural clay T = 296 K	11.09	[37]
T = 301 K	9.107	
T = 306 K	7.630	
Activated clay T = 296 K	18.86	
T = 301 K	15.45	
T = 306 K	12.51	
Multiwaled carbon nano materials two dimension (MWNT)	25.38	[38]
Multiwaled carbon nano materials one dimension (MWNTO)	19.608	
Multiwaled carbon (MWNT)	25.381	
Reduced graphene oxide (RGO)	22.27	
Multiwalled carbon nanotubes (MWCNT)	28.98	
Si(Mes)-(P)	4,210	This study
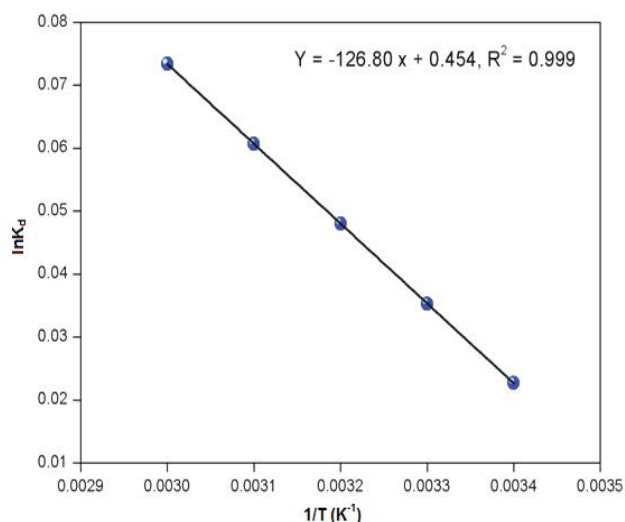
Fig. 14. Determination of thermodynamic parameters.

This study has given encouraging results, and we wish in the near future to carry out column adsorption tests under the conditions applicable to the treatment of industrial effluents.

4. Conclusion

The present study showed the successful preparation of activated carbon from mesoporous silica and perovskite and its efficiency as an adsorbent for the phenol removal from aqueous solution. Textural and surface characterizations of the adsorbent gave a BET surface of 450 m^2 g^{-1}. The adsorption capacity of phenol increased with increasing the phenol concentration and time; the kinetics indicated an optimum pH 4 and contact time of 60 min via three stages of adsorption kinetic profile. The phenol adsorption follows a pseudo-second-order kinetic model with determination coefficients R^2 very close to unity; which relies on the assumption that physisorption may be the rate-limiting step. The equilibrium adsorption data for the phenol onto Si(Mes)-(P) were analyzed by the different models, the results indicated that the Langmuir and Temkin models provide the best correlation.

The negative free enthalpy ($\Delta G°$) and positive enthalpy ($\Delta H°$) indicated that the phenol adsorption is spontaneous and endothermic over the studied temperatures range. The enthalpy clearly indicates a strong attachment of phenol to the adsorbent by forming a chemical bond and tends to find sites that maximize their coordination number with the surface. The negative entropy ($\Delta S°$) states clearly that the randomness increases at the solid-solution interface during the phenol adsorption onto Si(Mes)-(P), indicating that some structural exchange may occur among the active sites of the adsorbent. The comparison of the adsorption capacity of the prepared adsorbent with those reported in the literature show edits attractive properties from industrial and economic interests. Thus, overall, it can be concluded that activated carbon prepared would make a promising cost-effective adsorbent.

References

[1] A. Aygün, S. Yenisoy-Karakaş, I. Duman, Production of granular activated carbon from fruit stones and nutshells and evaluation of their physical, chemical and adsorption properties, Microporous Mesoporous Mater., 66 (2003) 189–195.

[2] I.O. Okeowo, E.O. Balogun, A.J. Ademola, A.O. Alade, T.J. Afolabi, E.O. Dada, A.G. Farombi, Adsorption of phenol from wastewater using microwave-assisted Ag–Au nanoparticle-modified mango seed shell-activated carbon, Int. J. Environ. Res., 14 (2020) 215–233.

[3] X.T. Liu, M.S. Wang, S.J. Zhang, B.C. Pan, Application potential of carbon nanotubes in water treatment: a review, J. Environ. Sci., 25 (2013) 1263–1280.

[4] K.P. Singh, A. Malik, S. Sinha, P. Ojha, Liquid-phase adsorption of phenols using activated carbons derived from agricultural waste material, J. Hazard. Mater., 150 (2008) 626–641.

[5] S.-H. Lin, R.-S. Juang, Adsorption of phenol and its derivatives from water using synthetic resins and low-cost natural adsorbents: a review, J. Environ. Manage., 90 (2009) 1336–1349.

[6] J.C. Lazo-Cannata, A. Nieto-Márquez, A. Jacoby, A.L. Paredes-Doig, A. Romero, M.R. Sun-Kou, J.L. Valverde, Adsorption of phenol and nitrophenols by carbon nanospheres: effect of pH and ionic strength, Sep. Purif. Technol., 80 (2011) 217–224.

[7] F.A. Banat, B. Al-Bashir, S. Al-Asheh, O. Hayajneh, Adsorption of phenol by bentonite, Environ. Pollut., 107 (2000) 391–398.

[8] A.T. Mohd Din, B.H. Hameed, A.L. Ahmad, Batch adsorption of phenol onto physiochemical-activated coconut shell, J. Hazard. Mater., 161 (2009) 1522–1529.

[9] M.T. Uddin, M.S. Islam, M.Z. Abedin, Adsorption of phenol from aqueous solution by water hyacinth ash, J. Eng. Appl. Sci., 2 (2007) 11–17.

[10] L.J. Kennedy, J.J. Vijaya, K. Kayalvizhi, G. Sekaran, Adsorption of phenol from aqueous solutions using mesoporous carbon prepared by two-stage process, Chem. Eng. J., 132 (2007) 279–287.

[11] R. Lafi, I. Montasser, A. Hafiane, Adsorption of congo red dye from aqueous solutions by prepared activated carbon with oxygen-containing functional groups and its regeneration, Adsorpt. Sci. Technol., 37 (2019) 160–181.

[12] S.K. Theydan, M.J. Ahmed, Adsorption of methylene blue onto biomass-based activated carbon by FeCl$_3$ activation: equilibrium, kinetics, and thermodynamic studies, J. Anal. Appl. Pyrolysis, 97 (2012) 116–122.

[13] M. Abbas, S. Kaddour, M. Trari, Kinetic and equilibrium studies of cobalt adsorption on apricot stone activated carbon, J. Ind. Eng. Chem., 20 (2014) 745–751.

[14] Z. Harrache, M. Abbas, T. Aksil, M. Trari, Thermodynamic and kinetics studies on adsorption of Indigo Carmine from aqueous solution by activated carbon, Microchem. J., 144 (2019) 180–189.

[15] M. Abbas, A. Cherfi, S. Kaddour, T. Aksil, Adsorption in simple batch experiments of Coomassie blue G-250 by apricot stone activated carbon—kinetics and isotherms modelling, Desal. Water Treat., 57 (2016) 15037–15048.

[16] C. Arora, D. Sahu, D. Bharti, V. Tamrakar, S. Soni, S. Sharma, Adsorption of hazardous dye crystal violet from industrial waste using low-cost adsorbent *Chenopodium album*, Desal. Water Treat., 167 (2019) 324–332.

[17] N. Sarker, A.N.M. Fakhruddin, Removal of phenol from aqueous solution using rice straw as adsorbent, Appl. Water Sci., 7 (2017)1459–1465.

[18] B.H. Hameed, A.A. Rahman, Removal of phenol from aqueous solutions by adsorption onto activated carbon prepared from biomass material, J. Hazard. Mater., 160 (2008) 576–581.

[19] G. Øye, J. Sjöblom, M. Stöcker, Synthesis, characterization and potential applications of new materials in the mesoporous range, Adv. Colloid Interface Sci., 89–90 (2001) 439–466.

[20] J. Roggenbuck, G. Koch, M. Tiemann, Synthesis of mesoporous magnesium oxide by CMK-3 carbon structure replication, Chem. Mater., 18 (2006) 4151–4156.

[21] J.F. Carneiro, J.R. Silva, R.S. Rocha, J. Ribeiro, M.R.V. Lanza, Morphological and electrochemical characterization of Ti/$M_xTi_ySn_zO_2$ (M = Ir or Ru) electrodes prepared by the polymeric precursor method, Adv. Chem. Eng. Sci., 6 (2016) 364–378.

[22] Z. Harrache, M. Abbas, T. Aksil, M. Trari, Modeling of adsorption isotherms of (5,5'-disodium indigo sulfonate) from aqueous solution onto activated carbon: equilibrium, thermodynamic studies, and error analysis, Desal. Water Treat., 147 (2019) 273–283.

[23] M. Abbas, Z. Harrache, M. Trari, Removal of gentian violet in aqueous solution by activated carbon equilibrium, kinetics, and thermodynamic study, Adsorpt. Sci. Technol., 37 (2019) 566–589.

[24] M. Abbas, T. Aksil, M. Trari, Removal of toxic methyl green (MG) in aqueous solutions by apricot stone activated carbon – equilibrium and isotherms modeling, Desal. Water Treat., 125 (2018) 93–101.

[25] Ü. Geçgel, O. Üner, G. Gökara, Y. Bayrak, Adsorption of cationic dyes on activated carbon obtained from waste *Elaeagnus stone*, Adsorpt. Sci. Technol., 34 (2016) 512–525.

[26] M. Hajjaji, S. Kacim, A. Alami, A. El Bouadili, M. El Mountassir, Chemical and mineralogical characterization of a clay taken from the Moroccan Meseta and a study of the interaction between its fine fraction and methylene blue, Appl. Clay Sci., 20 (2001) 1–12.

[27] M. Hesse, H. Meier, B. Zeeh, Spectroscopic Methods in Organic Chemistry, Georg Thieme Verlag, 2014.

[28] S. Lagergren, About the theory of so-called adsorption of soluble substances, Kungliga Svenska Vetenskapsakademiens Handlingar, 24 (1898) 1–39.

[29] Y.S. Ho, G. McKay, Pseudo-second order model for sorption processes, Process Biochem., 344 (1999) 51–65.

[30] N. Khalid, S. Ahmad, A. Toheed, J. Ahmed, Potential of rice husks for antimony removal, Appl. Radiat. Isot., 52 (2000) 30–38.

[31] I. Langmuir, The adsorption of gases on plane surfaces of glass, mica and platinum, J. Am. Chem. Soc., 40 (1918) 1361–1403.

[32] H. Freundlich, Concerning adsorption in solutions, Z. Phys. Chem. Stoch., 57 (1906) 385–470.

[33] M. Temkin, V. Pyzhev, Kinetics of ammonia synthesis on promoted iron catalysts, Acta Phys. Chim. URSS, 12 (1940) 327–356.

[34] M. Abbas, M. Trari, Kinetic, equilibrium and thermodynamic study on the removal of congo red from aqueous solutions by adsorption onto apricot stone, Process Saf. Environ. Prot., 98 (2015) 424–436.

[35] M. Abbas, M. Trari, Removal of methylene blue in aqueous solution by economic adsorbent derived from apricot stone activated carbon, Fibers Polym., 21 (2020) 810–820.

[36] E. El Gaidoumi, A. Chaouni Benabdellah, A. Lahrichi, A. Kherbeche, Adsorption of phenol in aqueous medium by raw and treated maroccan pyrophyllite, J. Mater. Environ. Sci., 6 (2015) 2247–2259.

[37] M. Djebbar, F. Djafri, M. Bouchekara, A. Djafri, Adsorption of phenol on natural clay, Appl. Water Sci., 2 (2012) 77–86.

[38] M. de la Luz-Asunción, V. Sánchez-Mendieta, A.L. Martínez-Hernández, V.M. Castaño, C. Velasco-Santos, Adsorption of phenol from aqueous solutions by carbon nanomaterials of one and two dimensions: kinetic and equilibrium studies, J. Nanomater., 2015 (2015) 1–14, https://doi.org/10.1155/2015/405036.